ISSN 2786-7102 (Online), ISSN 2786-7633 (Print)
https://doi.org/10.15407/srenergy2025.01.085

UDC 620:9

Ihor Bohachev[1]*, PhD (Engin.), Senior Researcher, https://orcid.org/0000-0001-7781-5767
Oleh Kozyr[2], PhD (Engin.), Associate Professor, https://orcid.org/0000-0002-9285-5940
Stanislav Sozonov[1], https://orcid.org/0000-0002-7584-4529
[1]General Energy Institute of NAS of Ukraine, 172, Antonovycha St., Kyiv, 03150, Ukraine;
[2]National Technical University of Ukraine "Igor Sikorsky Kyiv Polytechnic Institute", 37, Beresteiskyi Prosp., Kyiv, 03056, Ukraine
*Corresponding author: biv_vdoe@ukr.net

REDUCING THE INFLUENCE OF NOISE ON THE ACCURACY OF ULTRASONIC PULSE ONSET DETECTION

Abstract. *An essential component of ultrasonic nondestructive testing is determining the delay time between the transmitted and received signals. Therefore, the accuracy of determining the onset of both the transmitted and received pulse affects the accuracy of all subsequent calculations. The main measuring transducers are usually piezoelectric. A relatively new approach involves using small-aperture magnetostrictive transducers as a generator and receiver of the ultrasonic signal. Such magnetostrictive sensors have low-current excitation coils, resulting in low amplitudes of received signals. Therefore, it is an urgent task to develop algorithms for determining the onset of a pulse that could reduce the noise present in the signal or not be sensitive to it. In this paper, a method for determining the onset of an ultrasonic pulse is proposed based on utilizing a standard function from the LabVIEW library to determine the position of the peak value of a periodic pulse. The mathematical expressions for modeling transmitted and received pulses were obtained. Based on these mathematical expressions, a modeling experiment was conducted to verify the accuracy of determining the beginning of the probing pulse by the proposed method. The simulation experiment was performed with noise following a Gaussian distribution for the range of standard deviation (SD) values from 0 to 10. According to the modeling results, it was found that the proposed method allows determining the beginning of the probing pulse with a relative error not exceeding 3.5 % for the values of the SWR less than 2.*
Keywords: ultrasonic signal, magnetostrictive sensor, signal-to-noise ratio.

1. Introduction

One of the most common methods of controlling the properties of products in production is non-destructive testing [1]. Ultrasonic non-destructive testing is especially widely used. This method uses an acoustic signal to probe the sample under test. In this case, both the pulse sent and the reflected from the interference are measured.

noise and are used in medical ultrasound image processing. In addition, in images used for biomedical purposes, digital image processing methods are widely used to de-noise them [4]. In the paper [5], the Wavelet transform algorithm for noise filtering was proposed and its efficiency was evaluated on 292 images. The results obtained in [5] indicated that the effectiveness of the application of Wavelet transform algorithms depends on the selected filter parameters and their values, the ultrasonic signals themselves and the types of noise. And the algorithm proposed in the paper [6] based on the orthonormal wavelet family was tested on 110 images and showed its effectiveness.

A feature of the medical use of ultrasound signals is that the probing pulse is actively absorbed by the tissue, and the increase in the intensity of the pulse is limited by medical indicators [7]. Therefore, the reflected signal has a small amplitude value and signal-to-noise ratio. In the paper [7], the use of neural network methods of signal processing to reduce noise and improve the signal-to-noise ratio is proposed.

Recently, the use of blind source separation techniques for filtering ultrasound images has become quite popular [8]. At the heart of these algorithms is an approach that attempts to decompose the received signal into the components of which it might have been composed. At the same time, a feature of this algorithm is that it tries to separate a useful signal or a combination of signals and noises with minimal initial information about them. Accordingly, the work [8] analyzed the effectiveness of using such methods.

One type of noise that distorts an ultrasonic image is diffuse reverberation, which occurs due to the presence of multiple reflections of the probing pulse before reaching the receiving sensor. The presence of this noise distorts the image and increases the error in determining the onset of the probing pulse [9]. In the paper [9], a denoising algorithm based on a 3D fully convolutional neural network was proposed. The disadvantage of this method is that it suppresses uncorrelated and low-amplitude signals. Therefore, it cannot be used to analyze the signal of magnetostrictive sensors.

As for ultrasonic non-destructive testing itself, one of the newest methods used for testing is phased array ultrasonic testing. It is used to assess the integrity of materials or structures. The use of this approach to test composite materials, with significant acoustic absorption, is accompanied by exposure to significant electrical noise [10]. In general, there is a significant demand for the use of composite materials in heavy-loaded structures in the aerospace industry, wind turbines, in the transport industry, medical equipment, etc. [11]. For such materials, it was proposed in [10] to use a time-varying filter empirical mode decomposition joint wavelet thresholding method to de-noise the sensing signal.

Noise reduction of ultrasonic echo-pulse signals is an important task in non-destructive testing in industry. The presence of significant noise and low signal-to-noise ratio are the main obstacle to obtaining accurate values of the start of the probing pulse [12]. The paper [12] proposes an algorithm for noise suppression when using non-destructive testing in production, which is based on a combination of several statistical methods of signal processing. In addition, to reduce the impact of noise on the received ultrasonic echo signal, signal processing methods based on wavelet functions are used, which allows to increase the signal-to-noise ratio [13]. In addition, a phase method for determining the probing impulse of magnetostrictive sensors against the background noise was developed [14]. This method [14] is based on the use of the discrete Hilbert transformation, which allows to determine the envelope and phase of signals.

Determining the beginning of the sent and received pulses determines the accuracy of the signal delay calculation and the determination of non-destructive testing parameters. Noise and interference prevent accurate pulse onset detection. There are two approaches to finding the onset of the pulse for a noisy signal. The first is to de-noise the signals, usually using statistical methods, and then the filtered signal is used to find the beginning of the pulse. This approach was applied in the works discussed above.

The second approach is to use algorithms to determine the onset of the pulse in the presence of noise in the signal. Since any signal filtering or denoising introduces certain distortions into the signal, and then the algorithm for determining the onset of the pulse introduces its own errors. The task is to try to find the beginning of the

impulse by its certain characteristic features without getting rid of the noise. Thus, in the paper [14], a method for determining the beginning of an ultrasonic signal for testing the integrity of structures is considered. In this work, the method of signal analysis using continuous wavelet transform preprocessing and machine learning algorithms was applied. The paper [15] examines the approximation of an ultrasound signal using the particle swarm optimization algorithm to determine the onset of the pulse. In the paper [16], a simpler approach to signal approximation based on the Levenberg-Marquardt optimizing algorithm was proposed.

This work is devoted to the second approach to determining the beginning of the probing pulse.

2. Probing pulse simulation

The process of ultrasonic non-destructive testing using low-aperture magnetostrictive sensors involves parallel measurement of the sent and reflected pulses [17]. The measurement process is performed over a specified time with a constant sampling rate. These measurements are performed using continuous signal sampling hardware from magnetostrictive sensors [18]. The resulting voltage values are stored in the form of arrays of real numbers. These are so-called time samples of the current voltage values at the output of magnetostrictive sensors.

The sampling simulation should reflect the basic parameters of the ultrasound signals. Usually, the duration of the measurement is much longer than the duration of both the sent and reflected signals combined. In addition, the measurement itself begins long before the probe pulse is sent, which makes it possible to determine the beginning of the pulse. Therefore, both samples contain both the probing pulse itself and regions with a complete absence of an informative signal. In the following, we will consider the sampling of the sent signal, but all of the above can be used for sampling with a reflected pulse.

The sample can be divided into three regions and described by the following expression [19]:

$$f(t) = \begin{cases} f_0(t), & 0 \le t < t_0 \\ f_T(t), & t_0 \le t < np \cdot T \\ f_0(t), & t_0 + np \cdot T \le t < t_d \end{cases}. \quad (1)$$

Descriptions of the values specified in (1), as well as those that will be found in the text below, are given in Table. 1. In addition, it provides their values that were used in the sample modeling.

Table 1. Variable values and descriptions

Parameter	Value	Description
$t_0, \mu s$	3	The target value of all measurements in non-destructive testing. Time of the onset of the probing pulse
$T, \mu s$	2	Pulse period
t_s, ns	20	Sampling period
$t_d, \mu s$	15	Measurement duration
np	2	Number of periods
A, V	6	Pulse amplitude
phase, radθ	0	Initial pulse phase

The three regions in expression (1) are described by three functions. In addition, these three areas differ in time ranges. The first region (1) does not carry an informative signal and is modeled by a function that returns zero values in the specified time range:

$$f_0(t) = 0. \quad (2)$$

The expression (2), regardless of the current value of the timestamp, returns a zero value. This expression will be used to create subarrays of the sample that simulate the absence of a probing pulse. According to (1), there are two such subarrays at the beginning and at the end of the sample. That is, two of the three regions represent the absence of the pulse.

The third region contains the pulse itself. The probing pulse was modeled by a harmonic signal, which can be described by the expression:

$$f_T(t) = Asin\left(2\pi\frac{1}{T}t + \theta\right). \quad (3)$$

The expressions (2) and (3) are represented for a continuous independent variable, i.e. time. In the calculations, discrete expressions are used to obtain samples. In this case, the time variable is a discrete quantity and is a uniform sequence with a constant step. This step is the time sampling period t_s of the signal (Table 1). Thus, the *nth* element of the array of zeros, based on the expression (2), will look like:

$$y_0[n] = f_0(t[n]) = 0. \quad (4)$$

Similarly, we get the value of the *nth* element of the array containing the probing pulse, based on (3):

$$y_T[n] = f_T(t[n]) = Asin\left(2\pi\frac{1}{T}t[n] + \theta\right). \quad (5)$$

The expression (5) was used to derive one period of the pulse. Since the number of periods was chosen to be $np = 2$ (Table 1), the second period was obtained by copying the first.

Since the sample is discrete, it has a limited number of values. In addition, it is necessary to determine the size of the sample subarrays that correspond to the corresponding areas (1).

The first region (1) corresponds to the time period $[0, t_0)$. Accordingly, we determine the size of the subarray using the sampling period t_s:

$$N_b = \frac{t_0}{t_s}. \quad (5a)$$

Based on (5a), we determine the value of the *nth* element of the time array of the first region:

$$t[nb] = nb \cdot t_s; nb \in \{0,1, \dots, N_b - 1\}. \quad (6)$$

Using (4) and (6), we obtain the expression of the current value of the array of the first area of the voltage sample:

$$y_{b0}[nb] = f_0(t[nb]) = 0. \quad (7)$$

The array of the second area contains the values of the probing pulse. The size of the array of one pulse period on the time interval [0, T) is:

$$N_T = \frac{T}{t_s}. \quad (8)$$

The corresponding time array of one pulse period based on (8) is determined from the expression:

$$t[nT] = nT \cdot t_s; nT \in \{0,1, \dots, N_T - 1\}. \quad (9)$$

The array of voltages of one period is calculated using (9):

$$y_T[nT] = f_T(t[nT]) = Asin\left(2\pi \frac{1}{T} t[nT] + \theta\right). \quad (10)$$

As already noted, the array of values of the probing pulse voltages is formed by concatenation of the array of one pulse period with itself.

The last third region is the array of zeros, which, like the first region, is calculated based on equation (4). To calculate the length of the array, it is necessary to take into account the time intervals of the previous two regions:

$$N_a = \frac{t_d - (np \cdot T + t_0)}{t_s}. \quad (11)$$

The time array of the third region based on (11) will be:

$$t[na] = na \cdot t_s; na \in \{0,1, \dots, N_a - 1\}. \quad (12)$$

The corresponding array of voltages of the third region on the voltage of the time array (12) is determined:

$$y_{a0}[na] = f_0(t[na]) = 0. \quad (13)$$

The final array of voltage values of the probing pulse is formed on the basis of the concatenation of the arrays of the three regions (7), (10), and (13), which can be described by the expression:

$$y[n] = y_{b0}[nb] + y_T[nT] + y_T[nT] + y_{a0}[na]. \quad (14)$$

The time array corresponding to (14) is calculated based on the sizes of the respective component arrays (5a), (8), and (11) and is calculated accordingly:

$$t[n] = n \cdot t_s; n \in \{0,1, \dots, (N_b + N_T + N_T + N_a) - 1\}. \quad (15)$$

Expressions (14) and (15) allow to simulate the measurement of the probing pulse and obtain a sample for testing the algorithms for finding the beginning of the pulse.

3. Implementation of the probing pulse modeling algorithm

3.1. Modeling the ideal sample

Using the graphical programming environment LabVIEW, virtual instruments (VIs) were developed to simulate the measurement of the probing pulse.

First of all, a VI was implemented that allows to sample an ideal probing pulse without noise. This sample was used to test the algorithm for determining the onset of the pulse. The front panel (FP) of the developed VI is shown in Fig. 1. The FP contains widgets for controlling the pulse and sample parameters (Table 1), and a waveform graph for displaying the resulting sample with an indication of the beginning of the simulated pulse (Fig. 1).

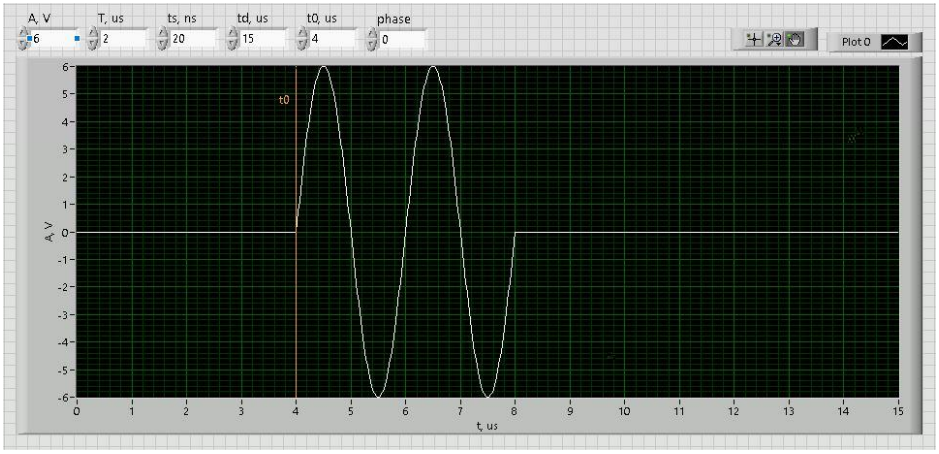

Figure 1. FP of the VI that models the probing pulse

The graphical code for the implementation of the algorithm for modeling an ideal sample of probing signal voltage values in the form of a block diagram (BD) is shown in Fig. 2.

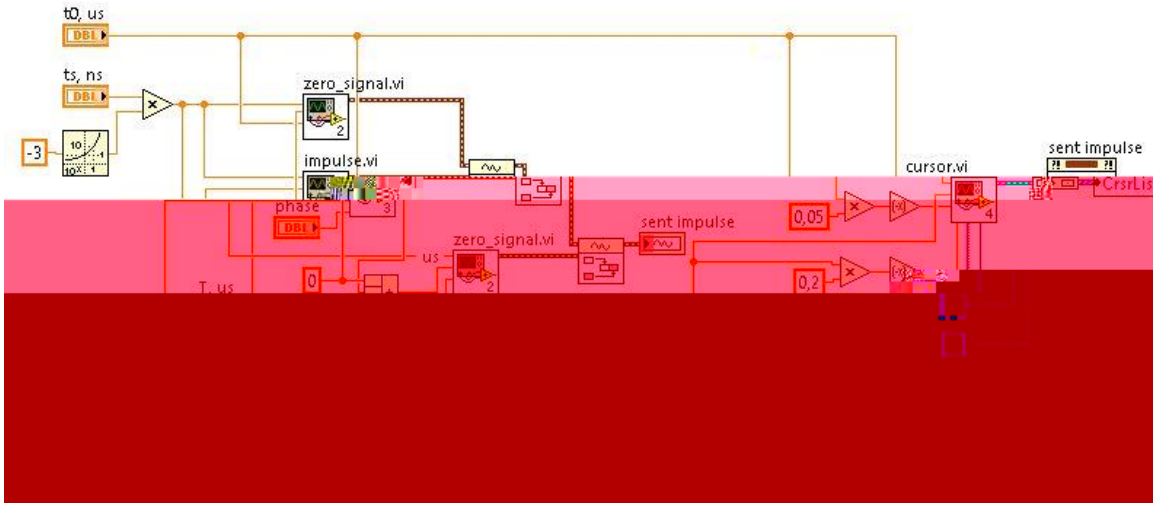

Figure 2. BD of the VI that models the probing pulse

This VI (Fig. 2) contains subVIs for implementing arrays of the corresponding three regions (1). The first and third regions of null values are created by subVI *zero_signal.vi*, which implements the generic expression (4) and expressions for the corresponding regions (7) and (13).

The probing pulse region based on expression (5) implements a *impulse.vi* that creates *np* pulse periods, according to expression (10).

The sizes of the corresponding time and voltage arrays according to (5a) and (8) are implemented in the corresponding subVIs. The size of the array of the third region (11) is implemented in the main VI (Fig. 2). In addition, the time arrays were not implemented separately, because the generated sample is stored using the *waveform* data type implemented by LabVIEW. This data type stores the array of signal values, the sample

period t_s and the measurement start time This data type is convenient because it does not consume the space of the computer's main memory to store an array of timestamp values. If you need such an array, for example, to display a signal on a graph, then a time array will be implemented.

The concatenation of the arrays in (14) is implemented in the main VI (Fig. 2). This VI will be used as subVI in other VIs elsewhere.

3.2. Modeling a sample with a noise

The following VI implements simulation of the measurement process (Fig. 3, Fig. 4). The FP of this VI contains an additional control the values of the standard deviation, *S, V* (Fig. 3). Real measurements are simulated by adding a random variable measurement error, interference, etc. to the ideal sample produced by VI in Fig. 2.

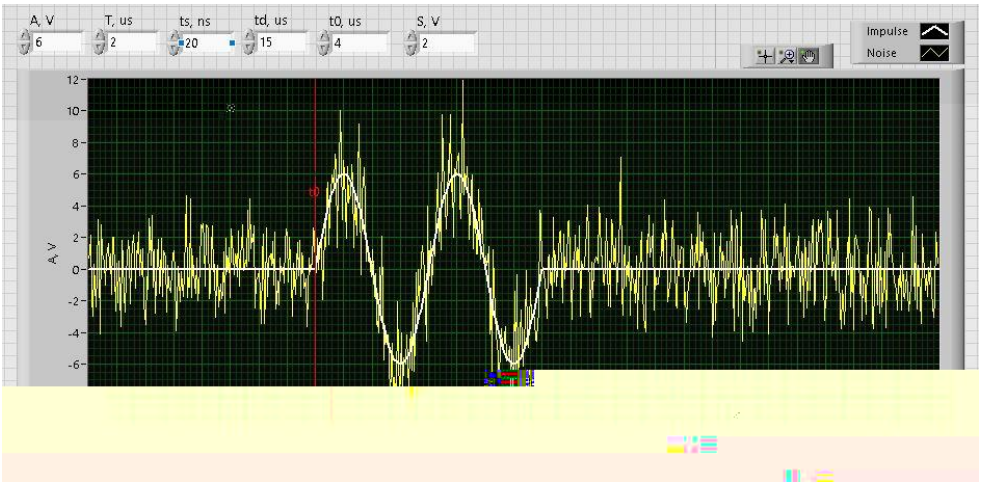

Figure 3. FP of the VI that models measured sample

For this work, a random variable is chosen with a normal law of distribution of possible values centered with a variable standard deviation, which is specified by the corresponding control (Fig. 3).

The VI (Fig. 4) forms an ideal sample based on subVI *impulse_simulation.vi*, which was considered earlier (Fig. 2).

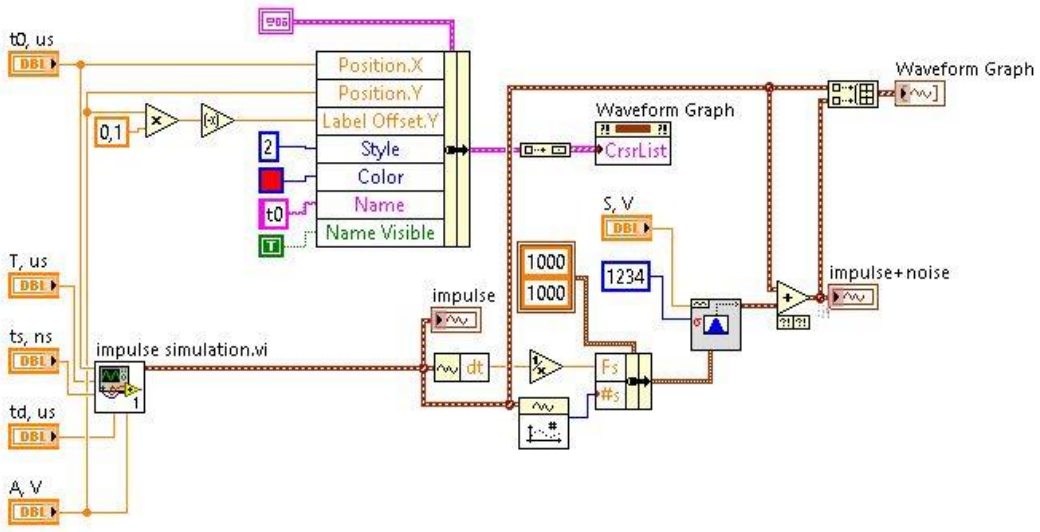

Figure 4. BD of the VI that models measured sample

The VI (Fig. 4) is the main one in the simulation of the measurement sample, which was used to determine the onset of the probing pulse.

3.3. Algorithm for determining the beginning of the probing pulse

To determine the beginning of the probing pulse, we will use the built-in *Pulse Measurements* VI [20], which belongs to the *Waveform Measurements* VIs palette. This VI is designed to analyze periodic signals and establish their characteristics: period, pulse width, duty cycle and pulse center of a selected pulse. FP of the VI (Fig. 5) contains two additional display elements: the defined value of the pulse start time *t0_fit* and the value of the relative error of its determination *dt0, %*.

Figure 5. FP of the VI that determines the start time of the pulse

To determine the beginning of the pulse, the pulse center parameter was taken as a basis. This parameter sets the time that corresponds to the peak of the pulse. Since this VI (Fig. 6) is designed for the analysis of periodic signals, it accordingly needs at least one period for analysis (the algorithm looks for the intersection of the midline line with a signal, and at the beginning of the pulse this intersection is absent), so the first positive half-period of the sine wave is skipped. In the case of a pr

In addition, the algorithm for determining the pulse center requires specifying the polarity of the pulse, that is, it will be a pulse containing rising and descending edges (high pulse) in relation to the midline or vice versa (low pulse). In Fig. 5, a high pulse (marked *t_center) was found*. Accordingly, an example of low pulse is shown in Fig. 7. The pulse center of the high pulse is calculated using the formula:

$$t_c = \frac{t_f - t_r}{2},$$

where t_r is the time of crossing the midline with a rising front; t_f the time of crossing the middle line with a falling front.

Finding the pulse center of the positive half-period of the second pulse period, it is possible to find the beginning of the pulse from the expression:

$$t_0 = t_c - T \cdot 1.25. \quad (16)$$

As can be seen from Fig. 5. This value is calculated without error for a perfect sample, without noise.

For the polarity of the low pulse, which is placed at 0.75 period relative to the beginning of the probing pulse, the expression (16) for calculating the beginning of the probing pulse will be as follows:

$$t_0 = t_c - T \cdot 0.75. \quad (17)$$

The result of using the expression (17) can be seen in Fig. 7.

Figure 7. Determination of the onset of pulse in the case of low pulse polarity

As in the case of high pulse for low pulse the algorithm determines the beginning of the pulse without error.

Next, the proposed pulse onset detection algorithm was tested for samples that simulate real measurements. The pulse onset detection algorithm used the high pulse polarity of Fig. 5 based on expression (16).

Thus, in the case when the standard deviation of Gaussian noise was 1/6 of the pulse amplitude, the measurement error was only <1 % (Fig. 8).

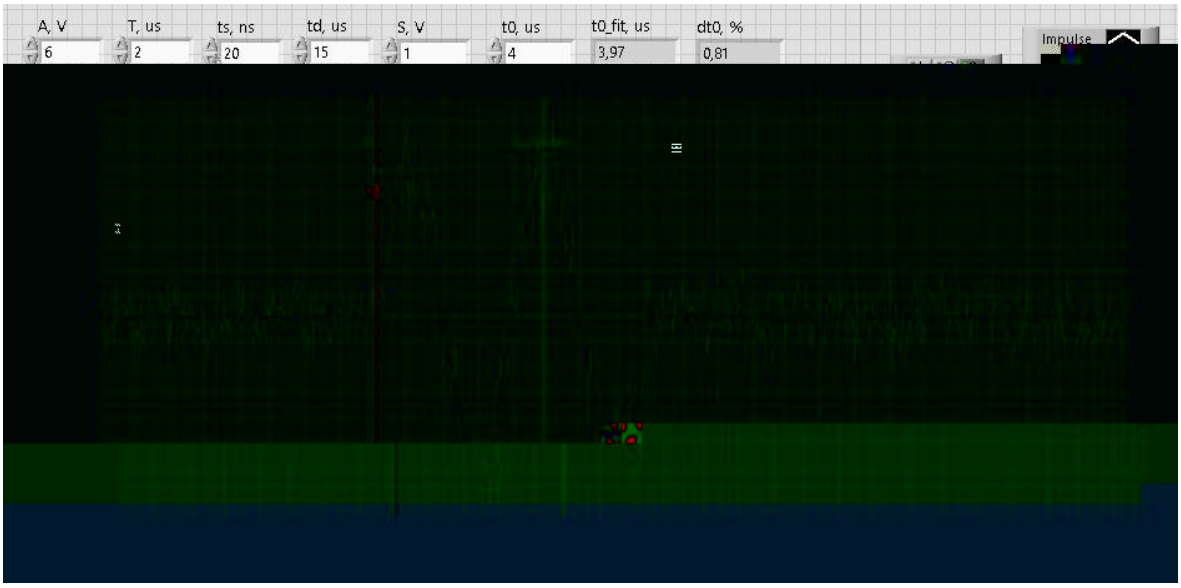

Figure 8. Determination of the onset of the pulse for a standard deviation equal to 1/6 of the pulse amplitude

For the case when the standard deviation of Gaussian noise was 2/3 of the amplitude of the pulse, the measurement error was almost 12 % (Fig. 9).

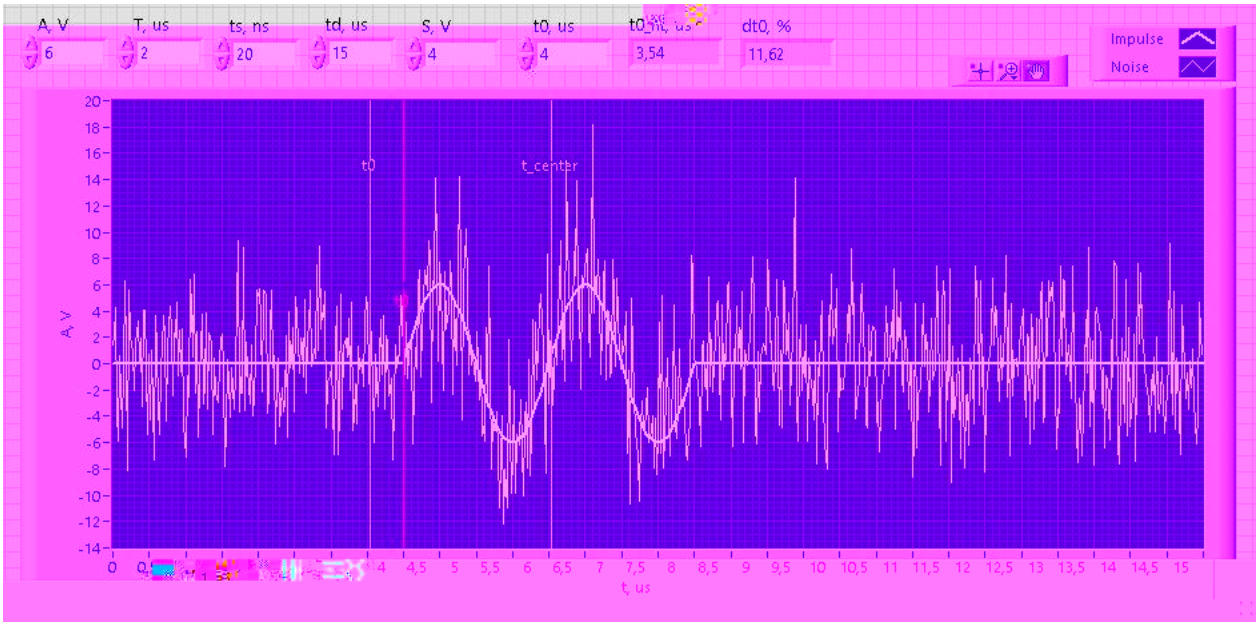

Figure 9. Determination of the origin of the pulse for a standard deviation equal to 2/3 of the pulse amplitude

4. Simulation experiment

To obtain a complete picture of the dependence of the error in determining the beginning of the probing pulse on the value of the noise standard deviation, VI was developed, which allowed iteratively obtaining an array of relative error values for an array of standard deviation in the range from 0 to 10 with a step of 0.5 (Fig. 10).

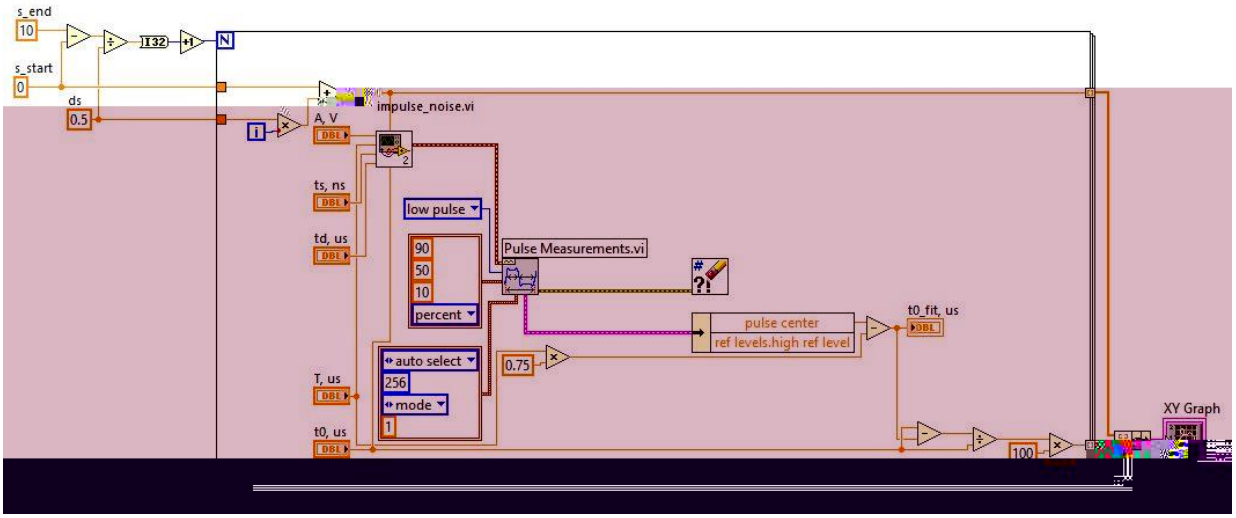

Figure 10. BD of the VI which iteratively determines the relative error in determining the origin of the pulse for different values of the standard deviation

The graph of the possible dependence of the error in determining the beginning of the sensing pulse by the proposed algorithm on the value of the noise standard deviation is shown in Fig. 11. As can be seen from the graph, small error values occur up to a PSF value of less than 2. Further, with increasing standard deviation, the error becomes significant, more than 100 %, and can change sign randomly.

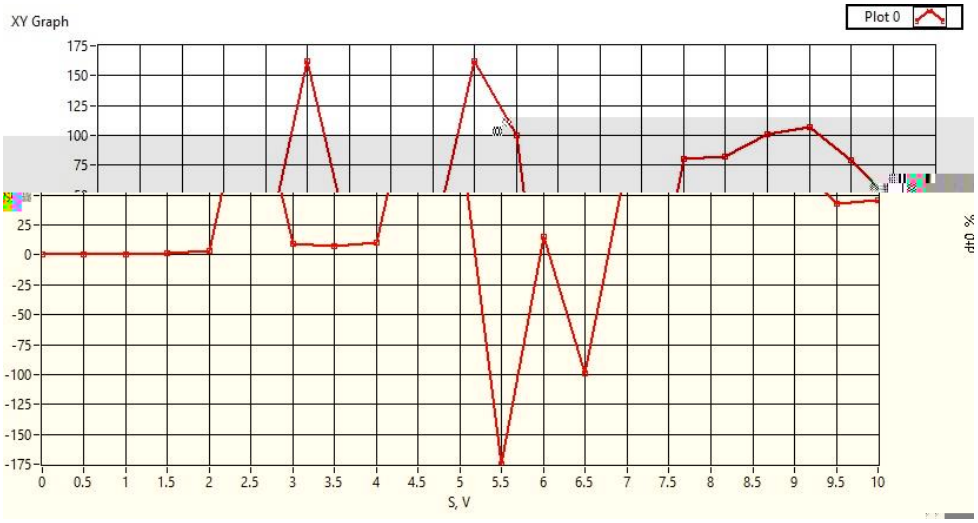

Figure 11. Graph of relative error values for determining the beginning of the sounding pulse by the proposed methods for the values of standard deviation

To verify the algorithm for determining the onset of a pulse based on the low pulse polarity, the VI shown in Fig. 10 was modified. A data stream was added to the loop with the algorithm for determining the beginning of the pulse based on the low pulse polarity (Fig. 7) based on expression (17). As a result, this VI (Fig. 12) returned pairs of error and standard deviation arrays.

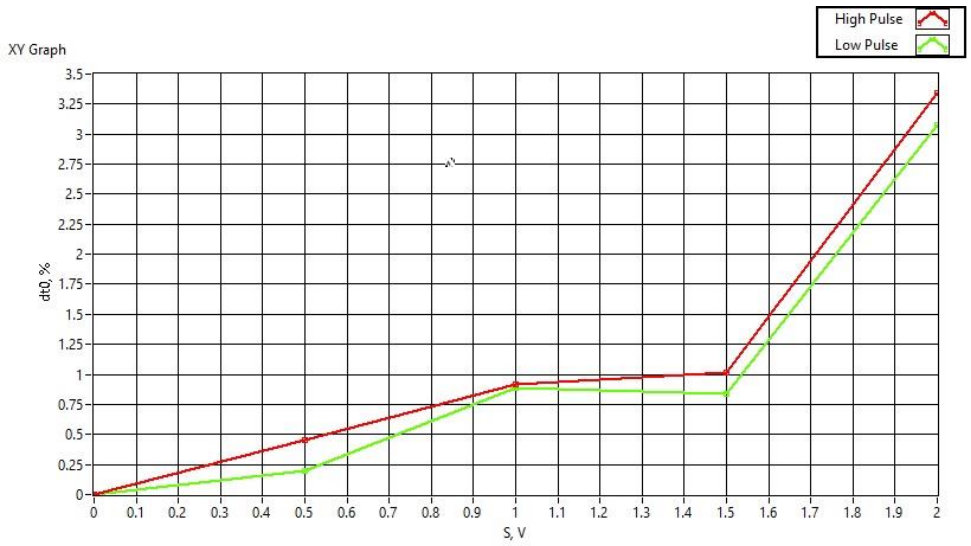

Figure 14. Graph of the dependence of the relative error of determining the onset of the pulse by the proposed method for two polarities on the standard deviation

As can be seen in Fig. 14, the use of the proposed method for determining the onset of the pulse has a lower relative error in the case of choosing the polarity of low pulse. However, the difference in relative errors in the two polarities is not significant, since it does not exceed 0.3 % in the range of standard deviation values from 0 to 2.

5. Conclusions

The paper proposes a method for determining the onset of the pulse of a probing ultrasonic signal, which is based on the use of a basic algorithm for determining the coordinate of the maximum of a certain periodic pulse, which is included in the library of the LabVIEW software development environment.

In the work, numerical simulations were performed using the proposed algorithm to determine the beginning of the probing pulse. The independent variable was the value of the noise standard deviation, which was selected in the range from 0 to 10. According to the results of the simulation, it was found that this algorithm allows to determine the beginning of the pulse with a relative error that does not exceed 3.5 %.

Mathematical expressions for modeling the probing pulse were also obtained in the work. The resulting mathematical apparatus will make it possible to simulate a probing pulse of any shape.

Author Contributions. Refinement of the methodology and study ideology, acquisition and analysis of research data I. Bohachev; signal modeling and development of data processing algorithms O. Kozyr; drafting of the preliminary manuscript and collection of research data S. Sozonov.

Funding.

References

1. Gupta, M., Khan, M. A., Butola, R., & Singari, R. M. (2021). Advances in applications of Non-Destructive Testing (NDT): A review. *Advances in Materials and Processing Technologies*, *8*(2), 2286 2307. https://doi.org/10.1080/2374068X.2021.1909332
2. Bohachev, I., Kovtun, S., Kuts, Yu., Sozonov, S., & Khaidurov, V. (2023). Enhanced phase method of signal detection for ultrasonic magnetostriction defectoscopy of power equipment. *System Research in Energy*, *2*(73), 72 82. https://doi.org/10.15407/srenergy2023.02.072
3. Duarte-Salazar, C. A., Castro-Ospina, A. E., Becerra, M. A., & Delgado-Trejos, E. (2020). Speckle Noise Reduction in Ultrasound Images for Improving the Metrological Evaluation of Biomedical Applications: An Overview. *IEEE*, 8, 15983 15999. https://doi.org/10.1109/ACCESS.2020.2967178

Анотація.

,

,

,

,5

Ключові слова: